

Effect of hysteretic constitutive models on elasto-plastic seismic performance evaluation of steel arch bridges

Tong Wang^{1a}, Xu Xie^{*1}, Chi Shen² and Zhanzhan Tang¹

¹College of Architecture & Civil Engineering, Zhejiang University, Hangzhou 310058, China

²International Project Group, Chodai Co., Ltd., Ibaraki 305-0812, Japan

(Received July 19, 2015, Revised January 9, 2016, Accepted January 11, 2016)

Abstract. Modified two-surface model (M2SM) is one of the steel elasto-plastic hysteretic constitutive models that consider both analysis accuracy and efficiency. However, when M2SM is used for complex strain history, sometimes the results are irrational due to the limitation of stress-strain path judgment. In this paper, the defect of M2SM was re-modified by improving the judgment of stress-strain paths. The accuracy and applicability of the improved method were verified on both material and structural level. Based on this improvement, the nonlinear time-history analysis was carried out for a deck-through steel arch bridge with a 200 m-long span under the ground motions of Chi-Chi earthquake and Niigata earthquake. In the analysis, we compared the results obtained by hysteretic constitutive models of improved two-surface model (I2SM) presented in this paper, M2SM and the bilinear kinematic hardening model (BKHM). Results show that, although the analysis precision of displacement response of different steel hysteretic models differs little from each other, the stress-strain responses of the structure are affected by steel hysteretic models apparently. The difference between the stress-strain responses obtained by I2SM and M2SM cannot be neglected. In significantly damaged areas, BKHM gives smaller stress result and obviously different strain response compared with I2SM and M2SM, and tends to overestimate the effect of hysteretic energy dissipation. Moreover, at some position with severe damage, BKHM may underestimate the size of seismic damaged areas. Different steel hysteretic models also have influences on structural damage evaluation results based on deformation behavior and low cycle fatigue, and may lead to completely different judgment of failure, especially in severely damaged areas.

Keywords: hysteretic constitutive model; modified two-surface model; steel arch bridge; fiber model; seismic response; damage evaluation

1. Introduction

When subjected to strong ground motions, long-span complex steel bridges such as steel arch bridges often experience complicated stress states. In the seismic design and analysis of these bridges, we can see that the full scale three-dimensional finite element is not frequently used due to its considerable computation cost and inconvenience to extract internal forces. On the opposite,

*Corresponding author, Professor, E-mail: xiexu@zju.edu.cn

^aPh.D. Student, E-mail: wangtong@zju.edu.cn

beam element is widely used as a numerical modeling method. Therefore, during the seismic analysis procedure of complex steel bridges, selected uniaxial stress-strain constitutive model of steel under cyclic loading forms the basis for further structural seismic response modeling (Shi *et al.* 2012).

Since the fluctuant axial forces of arch ribs under earthquakes could lead to complicated stress states, and play an important role in the seismic response of such bridges (Chavez and Alvarez 2008, Alvarez *et al.* 2012), the seismic performance evaluation of steel arch bridges attracts extensive concentrations from various researchers. Usami *et al.* (2004, 2005), Nonaka and Ali (2001), Chen *et al.* (2011), Liang and Chen (2010), Hu *et al.* (2015) studied the elasto-plastic seismic performance of steel arch bridges. Lu *et al.* (2004a, 2004b), Cetinkaya *et al.* (2006, 2009) studied the applicability of pushover analysis method in assessment of elasto-plastic seismic performance for steel arch bridges. To consider the impact of fluctuant axial forces, fiber beam method is used in these studies, and bilinear kinematic hardening model (BKHM) is adopted as stress-strain relationship. But in the studies mentioned above, effects of hysteretic models on the accuracy of elasto-plastic seismic response analysis on arch bridges have not been further compared. However, due to the complex stress features of steel arch bridges, the seismic behavior of such bridges may be more sensitive to hysteretic constitutive models. As a result, it is necessary to consider the effect of hysteretic models during the seismic performance evaluation of steel arch bridges.

In most current seismic design and evaluation of complex steel bridges, steel hysteretic stress-strain relationship is commonly defined as bilinear or tri-linear kinematic hardening model. But whether it gives a good prediction of the structures' cyclic behavior is still a question. There has only been a little discussion about this issue before. For example, Gao and Ge (2008), Goto *et al.* (1998) analyzed the hysteretic behavior of steel bridge piers using different hysteretic models. The comparison with experimental results showed that the calculation accuracy of BKHM for structural hysteretic energy dissipation capacity is not satisfactory. The same conclusion was drawn by Miyoshi *et al.* (2003) and Shi *et al.* (2012) through the analysis and experimental validation of steel arch ribs and a composite beam to steel column system subjected to cyclic loadings respectively.

Although BKHM is easy to use in seismic analysis, to characterize the cyclic behavior of the structural steel more accurately, various hysteretic models based on uniaxial specimen tests, such as multi-surface model proposed by Morz (1969), and two surface model proposed by Dalafalis and Popov (1975), have been proposed up to the present. Based on these hysteretic models, Shen *et al.* (1995) proposed the modified two-surface model (M2SM) to improve both the computational efficiency and accuracy. Its accuracy to analyze the hysteretic performance of steel bridge piers (Gao and Ge 2008, Usami *et al.* 2000 and Ge *et al.* 2009) and steel arch ribs (Miyoshi *et al.* 2003) subjected to cyclic loadings has been verified by experimental data. However, when M2SM was implemented under complex strain history, sometimes there were irrational stress calculating results that are obviously larger than the test results. The main reason for this defect is that at the critical point between elastic and plastic region (except for yield plateau), the plastic modulus E^p given by M2SM tends to be infinite. In fact, the test results showed that this assumption is not always satisfactory.

In this paper, the modification of stress-strain path judgment in different cases was improved to avoid this defect of M2SM, and the improved model is named improved two-surface model (I2SM) in this paper. Uniaxial specimens have been examined under cyclic loadings with small strain vibrations to verify the accuracy and applicability of the improved method. Based on this

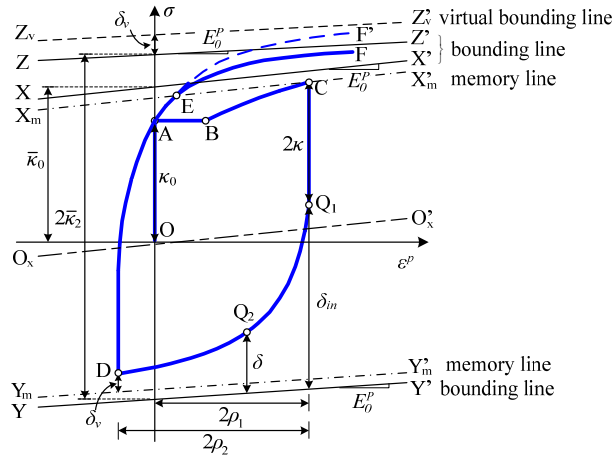


Fig. 1 Uniaxial cyclic stress σ -plastic strain ϵ_p curve of M2SM

modification, the elasto-plastic seismic response analysis of a deck-through type steel arch bridge with a 200 m long main span was conducted. In order to investigate the effects of different hysteretic models on the seismic performance evaluation of steel arch bridge, the results of improved two-surface model (I2SM) were compared with those of the modified two-surface model (M2SM), and bilinear kinematic hardening model (BKHM).

2. Improvement of the stress-strain path judgment of two-surface model

2.1 Brief introduction of modified two-surface model

First, the existing modified two-surface model proposed by Shen *et al.* (1995) will be briefly introduced. Fig. 1 shows the steel stress σ -plastic strain ϵ_p curve under uniaxial stress state. The loading point moves in elastic region from origin O to yield point A , then moves into the yield plateau AB , and then strain hardening stage BC . The elastic and plastic stage of the opposite side loading path is CQ_1 and Q_1D respectively. In the loading path Q_1D , the plastic modulus E^p is assumed as follows

$$E^p = \frac{d\sigma}{d\epsilon^p} = E_0^p + h \frac{\delta}{\delta_{in} - \delta} \tag{1}$$

where E_0^p is the slope of the corresponding bounding line YY' ; δ is the distance between the bounding line and loading point (such as point Q_2 in Fig. 1); δ_{in} is the value of δ at the initiation of a yielding process (such as point Q_1 in Fig. 1); h is called shape parameter.

To predict the hysteretic behavior of stress-strain curve, virtual bounding line and memory line were introduced in modified two-surfaced model. As shown in Fig. 1, in the prediction of path DEF , the bounding line is ZZ' , and the memory line is $X_m X'_m$, which is set to pass the point of maximum stress that the material has ever experienced (point C in Fig. 1). It is assumed that the memory line $X_m X'_m$ is parallel to the bounding line XX' for the current loading path. Suppose that

line $O_xO'_x$ is the center line of bounding line XX' and YY' , the the memory line $X_mX'_m$ and $Y_mY'_m$ will be assumed to be symmetric with line $O_xO'_x$ in tension and compression sides.

If the reversed loading point D in Fig. 1 does not reach the memory line $Y_mY'_m$, then assume that the distance between them is δ_v . In the prediction of the next path DEF, the virtual bounding line $Z_vZ'_v$ which is assumed to shift up the real bounding ZZ' by a distance δ_v will be used. The plastic modulus E^P is calculated as follows in the prediction of the path DE

$$E^P = E_0^P + h \frac{\delta + \delta_v}{\delta_{in} - \delta} \tag{2}$$

Once the loading point reaches the memory line (such as point E in Fig. 1), the plastic modulus E^P is calculated by Eq. (1) because the curve could not cross the real bounding line. Therefore the predicted path is DEF not DEF' in Fig. 1.

Furthermore, compared with the traditional two-surface model, more modification has been made in modified two-surface model as follows: (1) considers the reduction of elastic range κ and expansion of the radius of bounding surface $\bar{\kappa}$ with the increase of accumulated effective plastic strain $\bar{\epsilon}^p$; (2) considers the impact of stress history to yield plateau, and gives the rule to judge whether the yield plateau continues or disappears under cyclic loading; (3) the shape parameter h is thought to have a linear relationship with δ ; (4) considers the decrease of the slope of bounding line E_0^P in Eq. (1) with the increase of plastic work W^p .

2.2 Improvement of modified two-surface model

When the material experiences a complex cyclic loading history with small strain vibrations, at the critical point between elastic and plastic stage of a reloading path after unloading, the plastic modulus E^P given by Eq. (1) or Eq. (2) tends to be infinite in the following two cases, which obviously differs from the actual situation:

Case 1: The material is unloaded from plastic region to elastic region, and then reloaded to be yield again, that is the stress-plastic strain path O-A-B-C-B in Fig. 2.

Case 2: The material is unloaded from plastic region to elastic region, opposite-side loaded to plastic region with small plastic flow, then unloaded and opposite-side loaded again, that is the stress-plastic strain path O-A-B-C-D-E-F in Fig. 3.

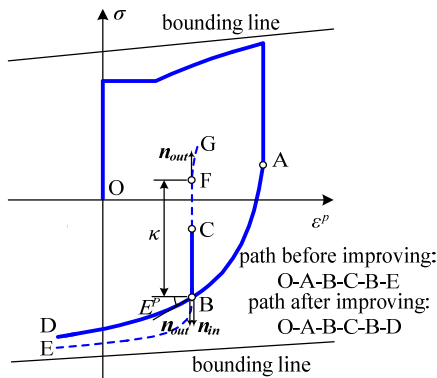


Fig. 2 Stress-plastic strain relation of Case 1

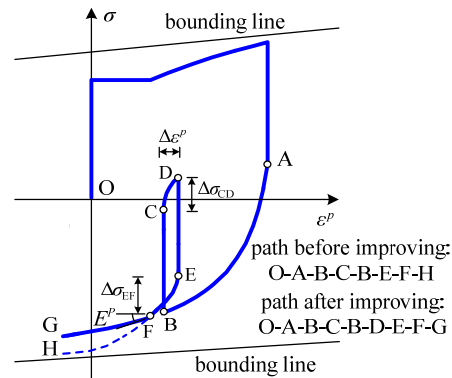


Fig. 3 Stress-plastic strain relation of Case 2

In this paper, improved method is proposed to avoid the calculation problem of plastic modulus E^P in the two cases mentioned above as follows.

Fig. 2 shows the strain variation path of Case 1. The material is unloaded from point B in plastic region to point C in elastic region, and in the following reloading path, point F and point B are defined as the yield point of “opposite-side reloading” and “same-side reloading” paths, respectively. According to the existing modified two-surface model, whether in “opposite-side reloading” or “same-side reloading” path, the plastic modulus E^P at point B or point F is infinity. But the actual situations were not like that. When the loading direction is “same-side reloading”, that is the path O-A-B-C-B, infinite E^P at point B is irrational. But when the loading direction is “opposite-side reloading”, that is the path O-A-B-C-F, it is realistic that E^P is infinity.

To avoid such problems, it is essential to distinguish the strain variation paths from yield points, and then determine E^P according to the reloading direction. The reloading direction can be judged by the normal vector \mathbf{n} of yield surface at point B or point F, which can be obtained as follows

$$\mathbf{n} = \frac{\sigma - \alpha_0}{\kappa} \tag{3}$$

where σ is the stress of loading point, and α_0 is the stress of elastic region center.

Assume that the normal vector \mathbf{n} of yield surface at the unloading point B is \mathbf{n}_{in} . In the following reloading path, when the loading point moves out of the elastic region, assume that the normal vector \mathbf{n} of yield surface at this point is \mathbf{n}_{out} . If $\mathbf{n}_{out} = \mathbf{n}_{in}$, then the loading point is at point B in Fig. 2, δ_{in} and δ_v in Eq. (2) should be identical to path AB, and obtained plastic modulus E^P should be equal to that of unloading point B. If $\mathbf{n}_{out} \neq \mathbf{n}_{in}$, then the loading point is at point F in Fig. 2, δ_{in} and δ_v in Eq. (2) should be updated according to the rules of existing modified two-surface model, and obtained plastic modulus E^P should be infinity. As shown in Fig. 2, after the improvement, the stress-plastic strain path has been changed from A-B-C-B-E to A-B-C-B-D, and the plastic modulus E^P at point B is no longer infinity.

Fig. 3 shows the strain variation path of Case 2. The material is unloaded from point B in plastic region and reloaded to point C in opposite plastic region, further loaded by a small plastic flow to point D, then unloaded and reloaded into plastic region again at point E. When moves into the elastic region, δ_{in} and δ_v at the reversed point B are defined as $\delta_{in,in}$ and $\delta_{v,in}$. The plastic strain and stress variation of path CD is assumed to be $\Delta \epsilon^P$ and $\Delta \sigma_{CD}$. When moves out of the elastic region, δ_{in} and δ_v at point E are defined as $\delta_{in,out}$ and $\delta_{v,out}$, which has been updated by the rules of modified two-surface model (as shown in Fig. 1). The plastic modulus E^P from point E is calculated through Eq. (2), until the stress variation $\Delta \sigma_{EF}$ (absolute value) from point E exceeds $\Delta \sigma_{CD}$ at point F in Fig. 3. δ_{in} and δ_v at point F can be evaluated as follows

$$\left. \begin{aligned} \delta_{in} &= (1-r)\delta_{in,in} + r\delta_{in,out} \\ \delta_v &= (1-r)\delta_{v,in} + r\delta_{v,out} \end{aligned} \right\} \tag{4}$$

where the coefficient r is used to define the small plastic flow of path CD

$$r = \frac{\|\Delta \epsilon^P\|}{\xi \frac{\sigma_y}{E}} \tag{5}$$

where σ_y is initial yield stress; E is elastic modulus; ζ is constant. Denominator value of Eq. (5) represents the limit of “small” plastic flow. Only when $0 \leq \nu \leq 1$ is the strain variation defined as “small”, and it is required to modify δ_{in} and δ_v through Eq. (4). ζ is assumed to be 2 in this paper. As can be seen in Fig. 3, after modifying Eq. (4) at point F, the following stress-plastic strain path FG is more rational than path FH. Similar to Case 1, loading directions of loading points can be judged by the normal vector of yield surface.

2.3 Model verification

After the improvement presented in this paper, the hysteretic model was named as improved two-surface model (I2SM) by us. To verify the computational accuracy and applicability of I2SM on material level, uniaxial experiments were carried out for specimens made of Q345qD steel under cyclic loading patterns with small strain vibrations. The Q345qD steel is commonly used for steel bridges in China. The Q345qD specimens were made into square section, as shown in Fig. 4(a). The Q345qD specimens were loaded in an INSTRON tension-compression machine with capacity of 25tonf as shown in Fig. 4(b). Strain was measured by tension and compression extensometer with a gauge length of 25 mm.

The hysteretic model was implemented into FEM software ABAQUS by its UMAT (User-defined material mechanical behavior) function. The two-surface material parameters of Q345qD steel were determined by a series of tests. The main parameters are shown in Table 1.

Fig. 5 presents the comparison between the tests of Q345qD specimens and analysis results. Specimen A and B were loaded under a loading path of Case 1, and specimen C and D were

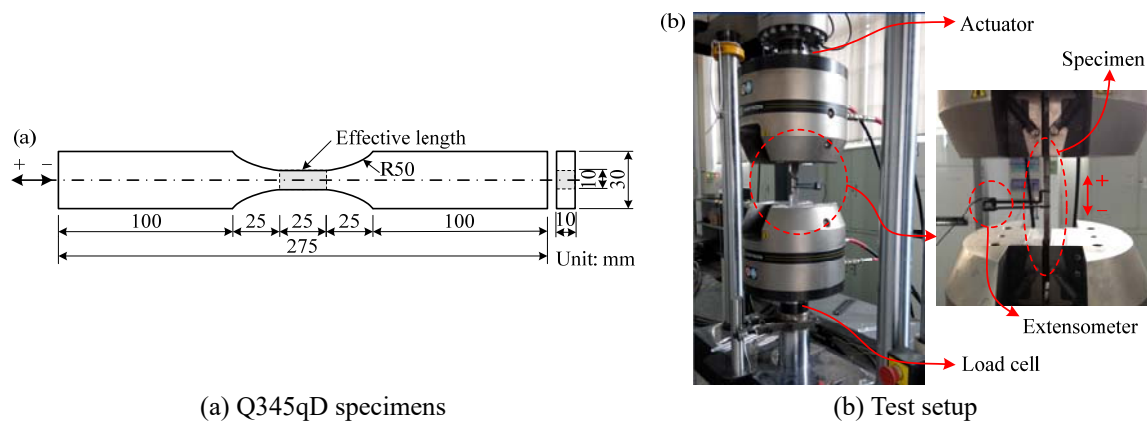


Fig. 4 Uniaxial tension-compression test

Table 1 Main model parameters of Q345qD and SM490 steel

Parameter	E / GPa	σ_y / MPa	μ	E_{st}^P / GPa	ε_{st}^P	σ_u / MPa	$\bar{\kappa}_0$ / MPa	E_{0i}^P / GPa
Q345qD	204.0	402.1	0.25	3.800	1.01×10^{-2}	552.7	425.0	2.550
SM490	210.0	381.0	0.29	5.060	1.88×10^{-2}	550.0	4.1	2.079

Note: E is elastic modulus; σ_y is initial yield stress; μ is Poisson’s ratio; E_{st}^P is the initial hardening plastic modulus; ε_{st}^P is the plastic strain at the end of yield plateau under monotonic loading; σ_u is ultimate strength

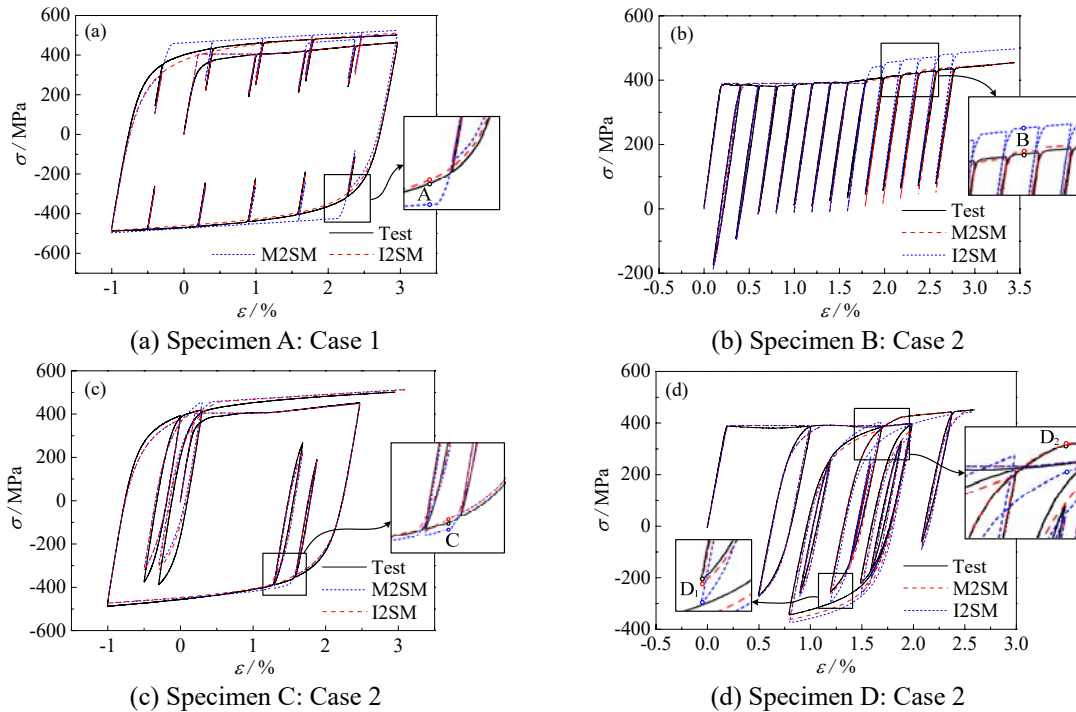


Fig. 5 Comparison between analysis and test results of Q345qD specimens

loaded under a loading path of Case 2. It can be seen from Fig. 5 that the stress-strain curve obtained by I2SM is closer to test results than that of M2SM, especially for Case 1, the result obtained by M2SM has significant error compared with test result due to overvalued E^P at every critical point. For example, at point A in Fig. 5(a) ($\varepsilon=2.1\%$), the relative error of stress obtained by M2SM reaches 21.9% compared with the test result, while that of I2SM is -3.8%. At point B in Fig. 5(b) ($\varepsilon=2.3\%$), the relative errors of stress obtained by M2SM and I2SM are 10.9% and 0.9% respectively. The improvement effect of Case 2 is not as obvious as that of Case 1 in general. In Fig. 5(c), at point C ($\varepsilon=1.4\%$), the relative errors of stress obtained by M2SM and I2SM are 4.8% and -1.2% respectively. In Fig. 5(d), due to the over-valuation of the stress at reserved point D₁ by M2SM, the stress in the next loading path is substantially underestimated, such as at point D₂ ($\varepsilon=1.2\%$), the relative error of stress obtained by M2SM reaches -9.7% compared with the test result, while that of I2SM is only 0.2%.

In order to further illustrate the necessity of the improvement in this paper on structural level, the hysteretic experiment curve of an unstiffened box steel column specimen conducted by Ge and Kang (2014) was taken for comparison. Fig. 6(a) and Fig. 6(b) show the analysis model and cross section of the specimen. Fiber model was used for quasi static analysis. Constant axial force $0.1N_y$ and cyclic displacement loading Δ were applied on top of the pier, where N_y is yield axial force. The random cyclic loading pattern is shown in Fig. 6(c). In the figure, Δ_y is yield displacement. The loading pattern is based on dynamic results of a real steel bridge pier subjected to the earthquake ground motion JRT-EW-M under the axial force ratio of 0.175. The specimen is made from Japanese structural steel SM490, and its main two-surface parameters are also listed in Table 1. Calculations were carried out based on both I2SM and M2SM respectively.

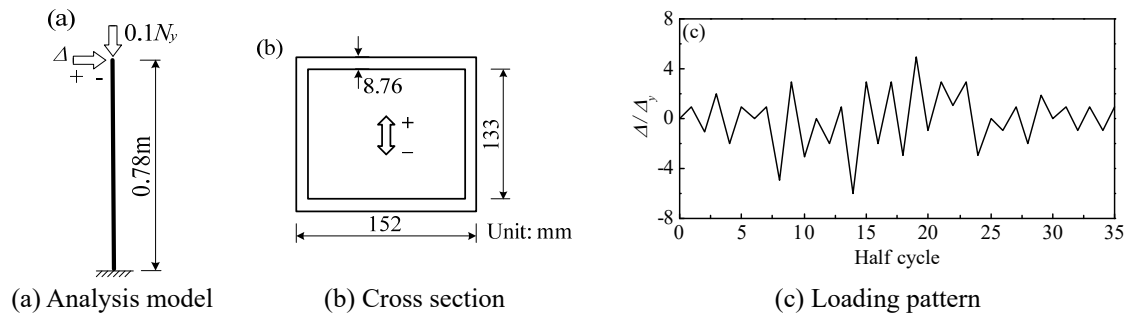


Fig. 6 Analysis model and loading pattern the unstiffened box steel column specimen

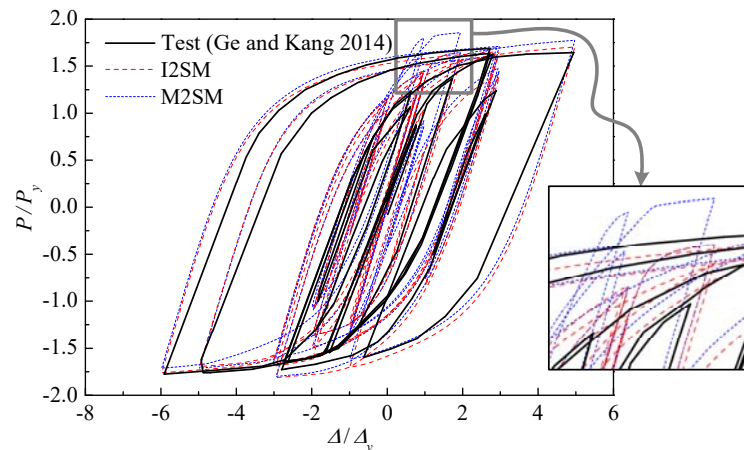


Fig. 7 Comparison results of hysteresis curve of the column specimen

Comparative results of horizontal load ratio P/P_y versus displacement ratio Δ/Δ_y curves on top of the specimen are shown in Fig. 7. It can be seen from the figure that under the random cyclic loading, M2SM would give overestimated prediction of the horizontal load due to the effect of overestimated E^p at critical points (see the amplified region in Fig. 7), while the prediction result obtained by I2SM agrees much better with the test curve. In general, a too plump hysteresis curve of the structure could be avoided in the reloading process using I2SM.

All the comparison above indicates that although M2SM gives generally good prediction of stress, when subjected to cyclic loading history with small strain vibrations, sometimes significant error will occur. I2SM could avoid the problem of M2SM in stress calculation, and more accurately reflects the hysteretic behaviors of steels under complex cyclic strain history.

3. Seismic response analysis model and ground motions

3.1 Overview of the bridge

In this section, a deck-through type steel arch bridge was taken as an example for elasto-plastic seismic response analysis. Fig. 8 shows the schematic view of the bridge with a 200 m-long span

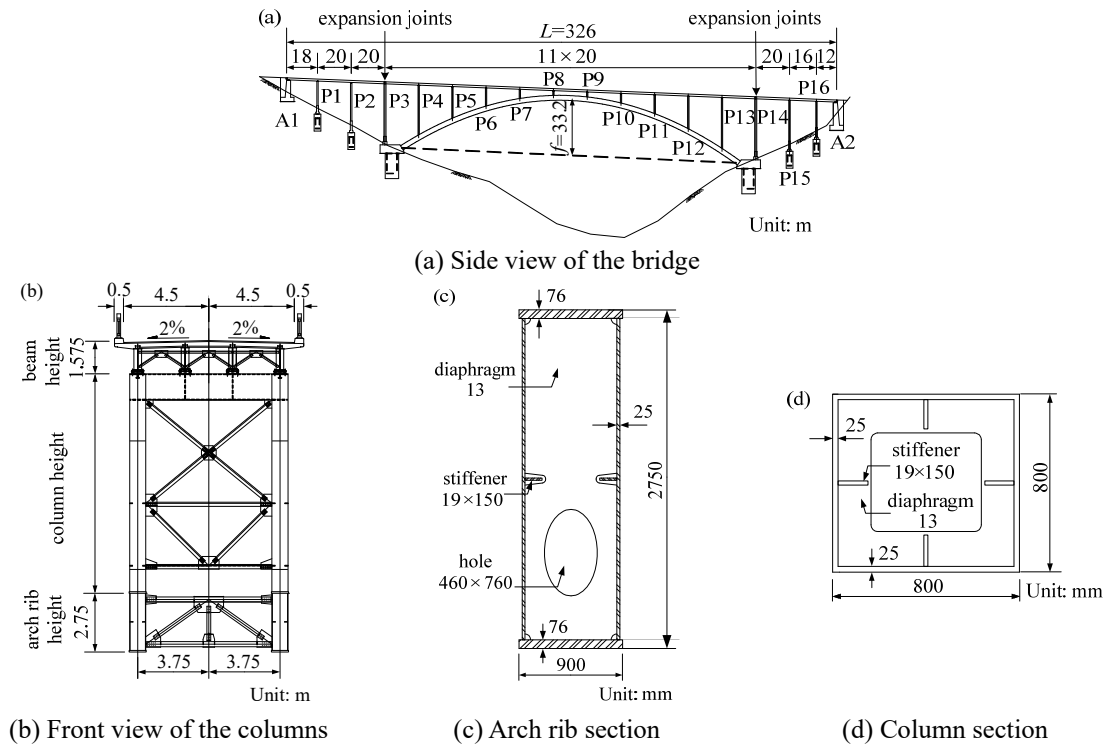


Fig. 8 Schematic view of the bridge

and a 10 m-wide deck. The deck consists of concrete slabs and 4 I-beams which are braced with lateral struts. The arch ribs are braced with lateral struts. The cross section of arch ribs is a single-cell box of 0.9 m \times 2.75m with a 76 mm-thick flange. The columns are of 0.8 m \times 0.8m square box with a 25 mm-thick plate. Among all the columns, P8 and P9 are fixed with arch ribs and girders at both ends and the rest are all fixed with arch ribs and pinned to the girders. The structure of P3~P14 were selected as object for seismic response calculation, since the expansion joints were set at both ends of those columns.

3.2 Analysis model

Fig. 9 shows the 3D seismic time-history analysis model of the bridge. Seismic damaged parts like arch ribs and columns were modeled by fiber model, and fiber division of the sections is shown in Fig. 9. The sectional fibers were 120 and 80 in number for the two sections. The fiber model was refined in the anticipated seismic damaged areas and the total number of elements is 2705. The deck and transverse braces were modeled by elastic beam elements as they do not suffer any damage from the earthquake. The concrete slab and 4 I-beams of the deck were simplified to a beam with tensile stiffness $EA=252$ GN, and in-plane and out-plane bending stiffness $EI_x=6.84$ GN \cdot m² and $EI_y=387$ GN \cdot m². The bearings were modeled by spring constraints between top transverse braces and the deck. The arch ribs were directly fixed on the ground and the abutments were not modeled. Soil-structure interaction was not considered in the analytical model. The initial stress of the bridge under dead load is imposed on the FEM model.

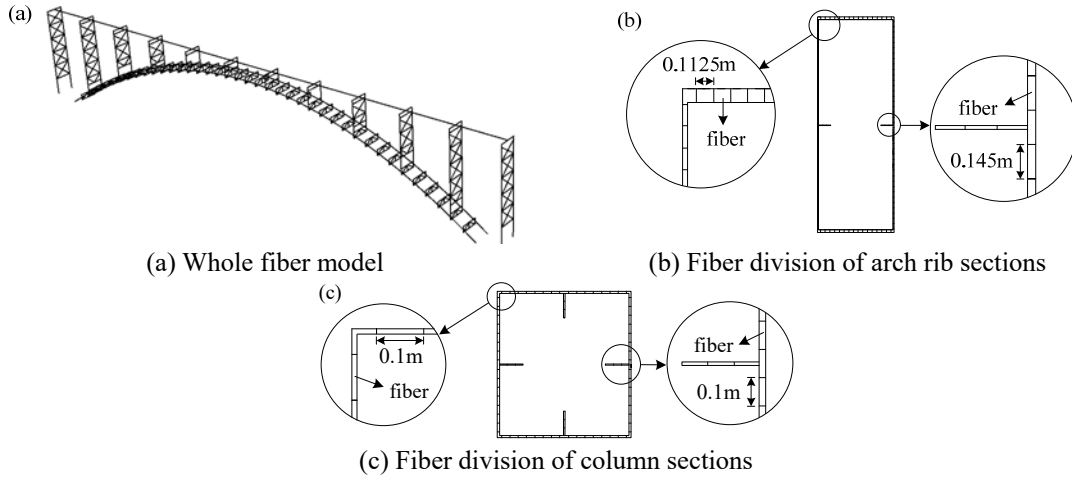


Fig. 9 Fiber model of the arch bridge structure

3.3 Define constitutive models in ABAQUS

FEM software ABAQUS was used in elasto-plastic seismic response analysis of the bridge. Three kinds of steel hysteretic models, I2SM, M2SM and BKHM, were utilized respectively. The initial yield strength of the steel is 356.7 MPa and the elastic modulus is 2.058×10^5 MPa. The Poisson's ratio is 0.25. Through ABAQUS's UMAT (User-defined material mechanical behavior) function, I2SM and M2SM were applied for the analysis. To make it easier to understand, the flow chart for I2SM is shown in Fig. 10, but it should be noticed that the flow chart only emphasizes on the improvement procedure in this paper. The detailed calculating method of the plastic module E^p and numerous parameters of two-surface model were not involved in the flow chart. The type of integration method we used is an implicit scheme.

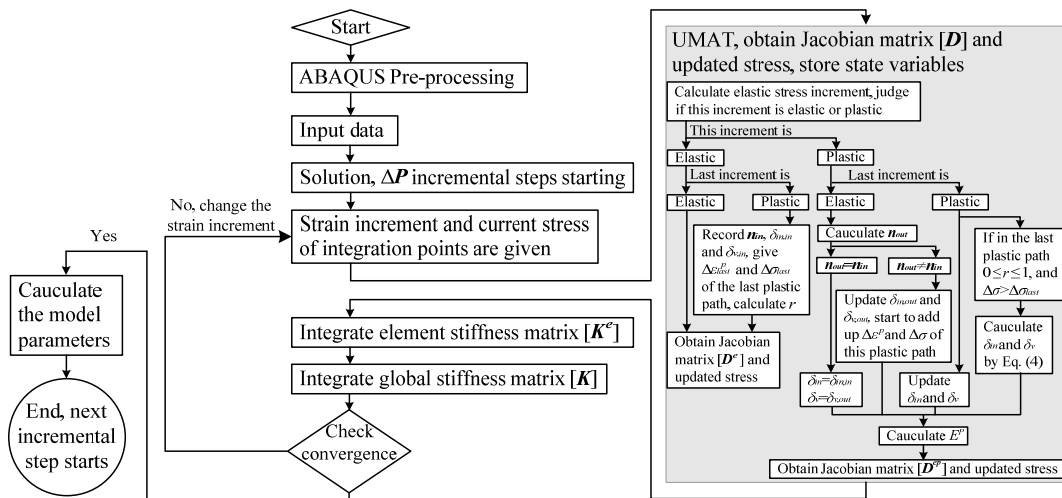


Fig. 10 Flow chart for I2SM in ABAQUS

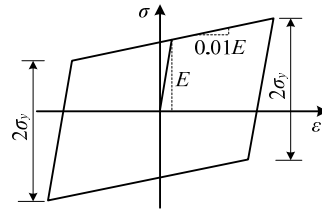


Fig. 11 Stress-strain relationship of BKHM

Table 2 Main model parameters of the bridge steel

E_{st}^P / GPa	ε_{st}^P	E_{0i}^P / GPa	$\bar{\kappa}_0$ / MPa	σ_u / MPa
6.997	1.24×10^{-2}	207.9	403.1	574.3

The stress-strain relationship of BKHM is shown in Fig. 11. The modulus after the yield point is taken as 1% of the initial one. Main two-surface model parameters of the steel are shown in Table 2.

3.4 Ground motions input

To make sure the occurrence of severe seismic damage and consider the randomness of ground motions, time-history analysis was carried out with Chi-Chi earthquake recorded near Sun Moon Lake (1999) and Niigata earthquake recorded in Ojiya (2004), both of which are near-fault earthquakes, as seismic inputs. Figs. 12 and 13 show the accelerograms and response spectra of Chi-Chi earthquake and Niigata earthquake, where a represents acceleration, t represents time, SA is acceleration response spectra value. Damping ratio of the response spectra is assumed to be 5%.

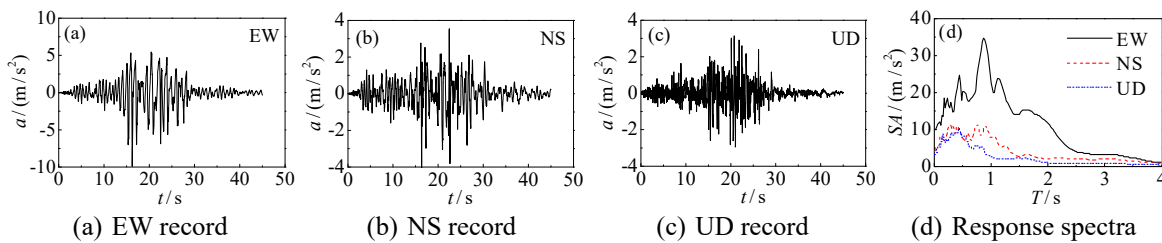


Fig. 12 Chi-Chi earthquake as ground motions input

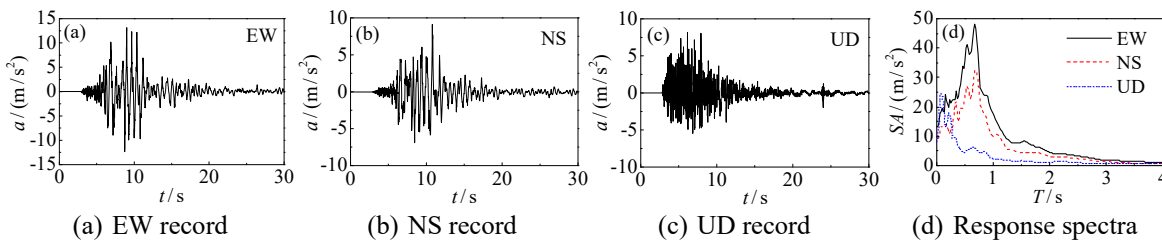


Fig. 13 Niigata earthquake as ground motions input

The peak acceleration of Chi-Chi earthquake and Niigata earthquake is 9.87 m/s^2 and 13.15 m/s^2 respectively. The EW, NS and UD records of the two earthquakes were taken as longitudinal, transverse and vertical excitation respectively. The two ground motions chosen here are entirely unrelated to actual seismic design of the bridge and they are selected just to make sure the occurrence of severe seismic damage simulation.

4. Comparison of seismic response

4.1 Comparison of displacement response

In view that the displacement response of the deck is greater than that of the arch ribs, the point on the deck at 1/4 span cross-section was selected for comparison. Figs. 14 and 15 show the comparison results of displacement responses under Chi-Chi earthquake and Niigata earthquake respectively, where d_{EW} , d_{NS} and d_{UD} indicate the longitudinal, transverse and vertical displacement responses. The maximum displacement comparison of the deck at 1/4 span is shown in Table 3. Results indicate that displacements obtained by the three hysteretic models are almost identical before the displacement reaches the peak value. With the increase of plastic deformation, small deviation gradually appears in the three curves. The displacement response obtained by BKHM slightly differs from that of I2SM and M2SM, especially in transverse direction. Overall, effect of hysteretic models on analysis accuracy of seismic displacement response is relatively small.

Table 3 Comparison of the maximum displacement

Direction	Chi-Chi Earthquake			Niigata Earthquake		
	d_{I2SM}/m	d_{M2SM}/m	d_{BKHM}/m	d_{I2SM}/m	d_{M2SM}/m	d_{BKHM}/m
Longitudinal	0.321	0.320	0.323	0.332	0.336	0.310
Transverse	0.396	0.396	0.380	0.223	0.225	0.212
Vertical	0.672	0.678	0.641	0.320	0.322	0.295

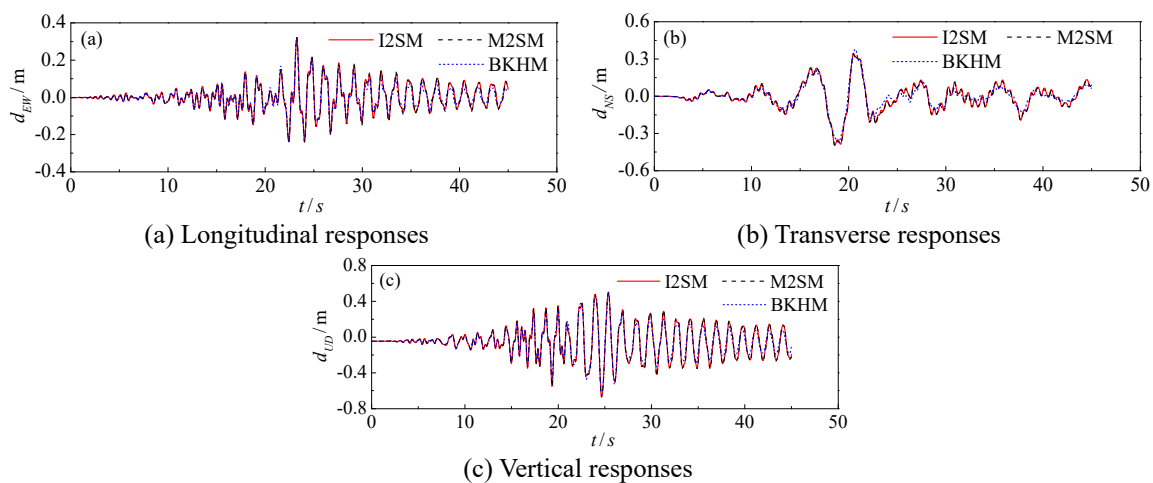


Fig. 14 Displacement time history curves of the deck at 1/4 span under Chi-Chi earthquake

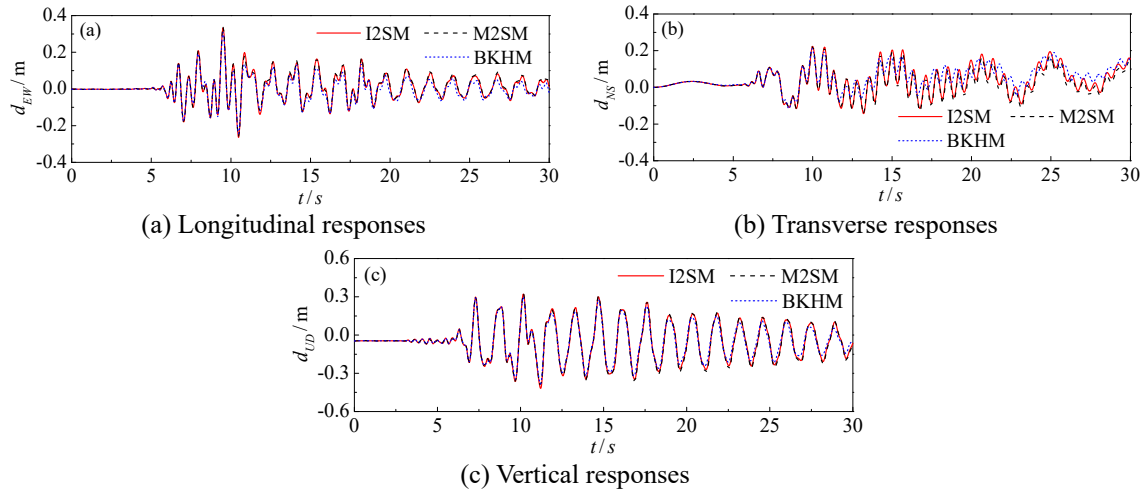


Fig. 15 Displacement time history curves of the deck at 1/4 span under Niigata earthquake

4.2 Comparison of axial force responses

The axial force comparison results of arch rib at 1/4 span under Chi-Chi earthquake and Niigata earthquake are shown in Fig. 16, where N is axial force responses, and N_y means yield axial force of the cross section. Table 4 gives the axial force range of the arch ribs at 1/4 span and the bottom of column P6, and tensile axial forces in the table are assumed to be positive. Table 4 reveals significantly fluctuant axial force effect on arch ribs of steel arch bridge under earthquakes. The maximum axial force of the arch ribs at 1/4 span can reach 0.37 times that of yield axial force under Chi-Chi earthquake. Results in Fig. 16 and Table 4 indicate that the axial force range obtained by BKHM is smaller than that of I2SM and M2SM.

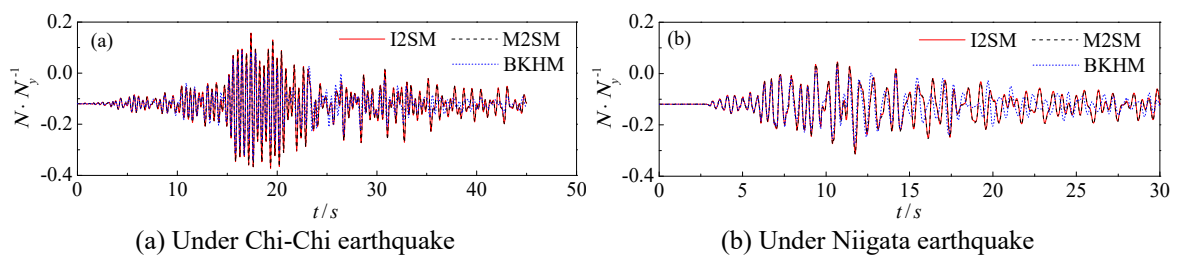


Fig. 16 Axial force responses of the arch ribs at 1/4 span

Table 4 Comparison of the axial force range

Section	Chi-Chi Earthquake			Niigata Earthquake		
	$N_{I2SM} \cdot N_y^{-1}$	$N_{M2SM} \cdot N_y^{-1}$	$N_{BKHM} \cdot N_y^{-1}$	$N_{I2SM} \cdot N_y^{-1}$	$N_{M2SM} \cdot N_y^{-1}$	$N_{BKHM} \cdot N_y^{-1}$
1/4-span arch rib	-0.37~0.16	-0.37~0.16	-0.34~0.09	-0.31~0.05	-0.31~0.05	-0.27~0.03
Bottom P6	-0.18~0.10	-0.18~0.10	-0.15~0.06	-0.12~0.06	-0.12~0.06	-0.13~0.05

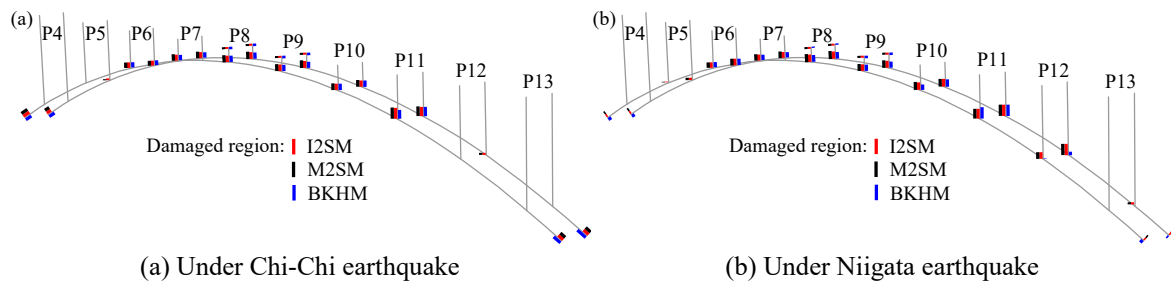


Fig. 17 Seismic damaged areas of the arch bridge

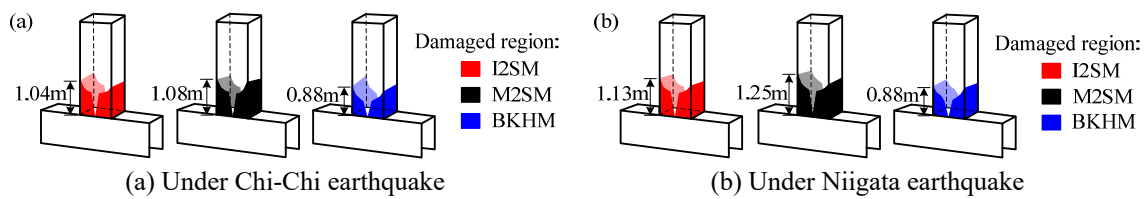


Fig. 18 Plastic region at the bottom of column P8

4.3 Comparison of seismic damaged areas

Fig. 17 shows the distribution of seismic damaged areas under Chi-Chi earthquake and Niigata earthquake. As it can be seen, seismic damaged areas obtained by the three hysteretic models mainly concentrate on the bottom of columns and the arch springings. The bottom of column P8 and P9 shows severe damage and only slight damage can be found in the rest damaged areas. The damage distributions obtained by the three hysteretic models are similar to each other, but have some difference in dimension, such as in the severely damaged areas at the bottom of column P8 and P9.

Fig. 18 shows the size of plastic region at the bottom of column P8. It can be seen from the figure that the size of seismic damaged areas obtained by I2SM and M2SM are larger than that of BKHM under different ground motions. When subjected to Niigata earthquake, the plastic length predicted by I2SM is 1.13 m, which is about 1.3 times of that of BKHM. The above results demonstrate that at some positions with severe damage, BKHM may underestimate the size of seismic damaged areas.

It should be noticed that fiber model has a lack of accuracy for the prediction of plastic regions. Due to the concern of computation cost, this paper has not modeled the seismic damaged areas by fine shell elements. Further study about this question will be conducted in future.

4.4 Comparison of Stress-strain history

For this bridge, plastic region at the joints of arch ribs and columns near the mid-span shows the most significant extension. The stress-strain hysteretic curves of the integration points with the maximum plastic strain at the bottom of column P6~P8 were taken as examples, as shown in Figs. 19 and 20. Due to symmetry of the bridge, results of column P9~P11 will no longer be displayed. In the figures, σ and σ_y represent stress and yield stress respectively; ε and ε_y are for strain and yield strain respectively.

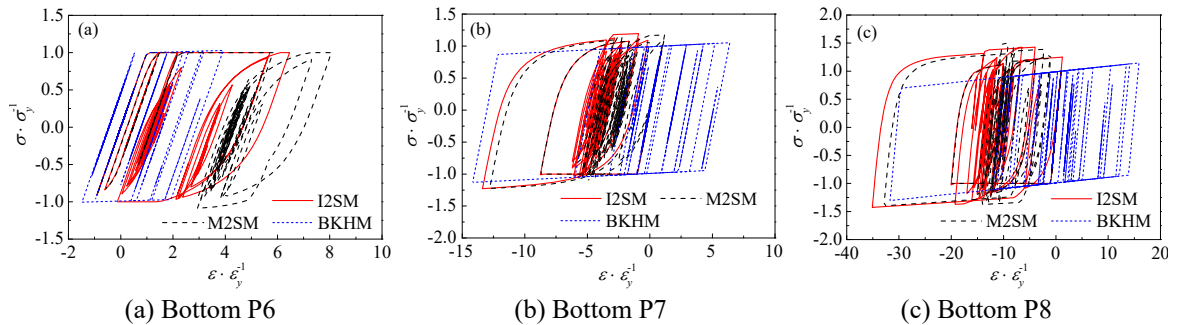


Fig. 19 Stress-strain hysteretic curves of some column bases under Chi-Chi earthquake

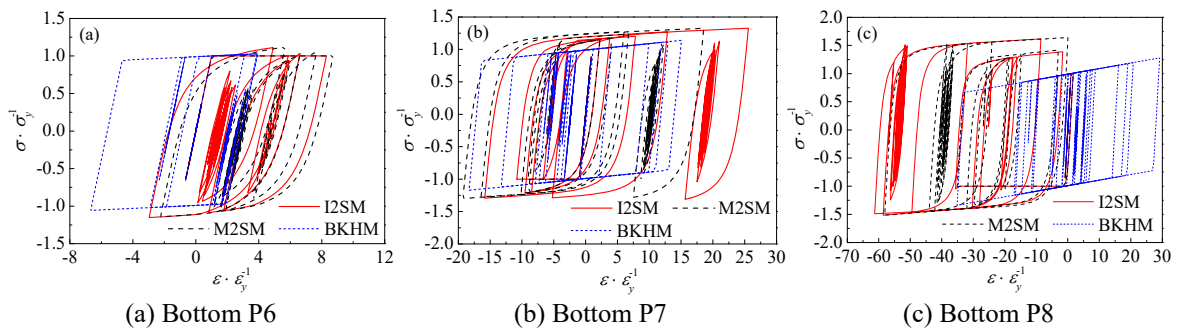


Fig. 20 Stress-strain hysteretic curves of some column bases under Niigata earthquake

Figs. 19 and 20 indicate that there are great differences between the stress-strain hysteretic curves obtained by the three models. The I2SM and M2SM results are much larger than BKHM results, especially in severely damaged areas. That is because of the consideration of expansion effect on the radius of bounding surface with the increase of accumulated effective plastic strain in two-surface models.

In addition to the differences of the stress results, the expansion of structural plastic strain also appears great differences due to different stiffness in plastic region between the models. The difference between the maximum compressive strain obtained by I2SM and M2SM at the bottom of column P7 under Chi-Chi earthquake can reach 3.2 times of yield strain, which should not be neglected. Due to the high natural frequency of arch bridges compared with other types of bridges with similar span, the strain responses also contain much high frequency components, which is small strain vibration. Therefore, I2SM could give more accurate results.

It also can be seen from Figs. 19 and 20 that the strain responses of BKHM have large difference compared with that of I2SM and M2SM. In severely damaged areas such as the bottom of column P8, under Niigata earthquake, the maximum strain obtained by I2SM at the bottom of column P8 is up to 60 times of yield strain, while the result of BKHM is only 35 times.

Table 5 shows the comparison of the hysteretic energy dissipation in the damaged areas mentioned above. W represents plastic work (the integral area of stress-strain hysteretic curve). As can be seen from the table, under different ground motions, the hysteretic energy dissipation results of BKHM are much higher than those of I2SM and M2SM at the bottom of column P8, where severely damaged, and the maximum relative error is over 50%. The results demonstrate

Table 5 Comparison of hysteretic energy

Section	Chi-Chi Earthquake			Niigata Earthquake		
	W_{I2SM}/MPa	W_{M2SM}/MPa	W_{BKHM}/MPa	W_{I2SM}/MPa	W_{M2SM}/MPa	W_{BKHM}/MPa
Bottom P6	9.9	9.1	4.3	21.5	22.0	22.4
Bottom P7	33.9	34.9	41.5	115.1	120.9	125.7
Bottom P8	113.0	103.9	177.4	243.8	235.8	273.2

that it is easy to overestimate the hysteretic energy dissipation effects of regions with significant plastic development based on BKHM.

In summary, hysteretic behavior of damaged areas of bridge is apparently affected by steel hysteretic constitutive models.

4.5 Effect on seismic damage evaluation: deformation behavior

Due to the good ductility of steel structures, for the seismic structural security demands of members allowing plastic deformation, failure of steel bridges always depends on two kinds of characteristics: deformation behavior and low cycle fatigue under strong earthquakes (Usami 2007). The index and requirements of the seismic performance evaluation method are listed in Table 6 as follows.

At present, there is no widely accepted checking method to determine the ultimate state of deformation behaviors based on fiber models. Based on numerous FEM simulations, Ge *et al.* (2004) suggested that the failure of steel column is usually determined by local buckling of steel plates, and the post-earthquake residual bearing capacity of the structures can be evaluated by a strain limit. According to this criterion, the ultimate state is thought to be reached when the average strain over the effective failure length at a critical place reaches the ultimate strain. The effective failure length L_e of a box-section member is assumed as (Usami 2007)

$$L_e = \min(0.7b, a) \quad (6)$$

where b is the flange width and a is the diaphragm spacing. Considering the effect of local buckling, an empirical formula for ultimate strain applying to fiber models of stiffened box-section columns was proposed by Ge *et al.* (2004), as follows

$$\frac{\varepsilon_u}{\varepsilon_y} = \frac{0.7}{(R_r \lambda_s^{0.18} - 0.18)^{1.3} (1 + N/N_y)^{2.2}} + \frac{3.2}{1 + N/N_y} \leq 20.0 \quad (7)$$

where ε_u is ultimate strain, ε_y is yield strain; N represents axial force; R_r is flange width-thickness

Table 6 Seismic security evaluation method for members allowing plastic deformation (Usami 2007)

Limit state	Behavior	Index	Evaluation ($S_d/R_d \leq 1.0$)	
			Response S_d	Limit R_d
Median	Deformation	Strain	Maximum strain response ε_{\max}	Ultimate strain ε_u
	Low cycle fatigue	Strain	Cumulative fatigue damage D	Limited fatigue damage=1.0

ratio parameter of the box section; λ_s is stiffener's slenderness ratio parameter. R_r and λ_s is defined by

$$R_r = \frac{b}{t} \sqrt{\frac{\sigma_y}{E} \frac{12(1-\mu^2)}{4\pi^2 n^2}} \tag{8}$$

$$\lambda_s = \frac{1}{\sqrt{Q}} \frac{a}{r_s} \frac{1}{\pi} \sqrt{\frac{\sigma_y}{E}} \tag{9}$$

where t is the thickness of the flange plate, n is the number of subpanels divided by stiffeners; r_s is radius of gyration of a T-shape cross-section consisting of one longitudinal stiffener and the adjacent subpanel of width b/n ; μ is passion ratio; and Q in Eq. (9) is defined by

$$Q = \frac{1}{2R_r} \left[\beta - \sqrt{\beta^2 - 4R_r} \right] \tag{10}$$

$$\beta = 1.33R_r + 0.868 \tag{11}$$

Eq. (7) is only applicable to sections with axial compressive ratio $0.0 \leq N/N_y \leq 1.0$, and width-thickness ratio parameter $0.3 \leq R_r \leq 0.5$.

The severely damaged column P7 and P8 were taken as examples to illustrate the effect of hysteretic models on seismic damage evaluation of the structure based on deformation behavior. Through calculation, it shows that width-thickness ratio parameter R_r of each column is 0.367, and slenderness ratio λ_s is 0.381, so Eq. (7) is valid for the cross sections. Fig. 21 shows the average strain and ultimate strain history of column P7 and P8. Considering that the axial force responses obtained by the three hysteretic models do not have large difference, only the axial force obtained by I2SM was used to calculate the ultimate strain through Eq. (7). Notice that the columns may develop tension forces under earthquake. While calculating the ultimate strain, if N is 0 or less, take $N=0$ to ensure the ultimate strain to take a safety value. The results of column P7 under Chi-Chi earthquake were not included because it's relatively small.

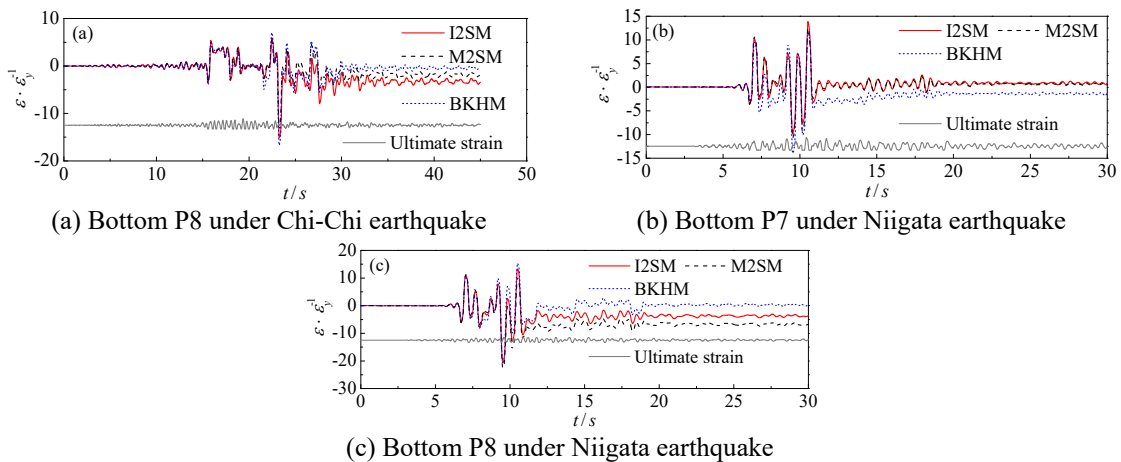


Fig. 21 Strain history of some column bases under Chi-Chi earthquake

Table 7 Maximum average compressive strain and corresponding ultimate strain of some columns

Earthquake	Section	I2SM		M2SM		BKHM	
		$\varepsilon_{max} \cdot \varepsilon_y^{-1}$	$\varepsilon_u \cdot \varepsilon_y^{-1}$	$\varepsilon_{max} \cdot \varepsilon_y^{-1}$	$\varepsilon_u \cdot \varepsilon_y^{-1}$	$\varepsilon_{max} \cdot \varepsilon_y^{-1}$	$\varepsilon_u \cdot \varepsilon_y^{-1}$
Chi-Chi	Bottom P8	-15.1	-12.5	-13.4	-12.5	-16.7	-12.5
Niigata	Bottom P7	-9.8	-12.3	-10.7	-12.2	-14.0	-12.2
	Bottom P8	-20.6	-12.5	-22.6	-12.4	-20.6	-12.3

Table 7 lists the maximum average compressive strain over the effective failure length strain ε_{max} and ultimate strain ε_u at corresponding time. As can be seen from the table, the maximum strain obtained by different hysteretic models exceeds its limit with different extent. In addition, according to the strain histories obtained by different hysteretic models, the judgment of failure may be completely different. For example, under Niigata earthquake, for column P7 shown in Fig. 21(b), BKHM predicts that the ultimate state reaches at $t=9.4$ s, while I2SM and M2SM predicts that failure will not happen till the end of the earthquake. In a word, strain histories obtained by different hysteretic models are obviously different, which has affected the structural seismic damage evaluation based on deformation behavior.

4.6 Effect on seismic damage evaluation: low cyclic fatigue

The seismic performance evaluation method proposed by Usami (2007) suggests that even if the structure does not reach the ultimate strain under earthquakes, ductile fracture may still happen due to low cyclic fatigue. Therefore, seismic damage evaluation of damaged regions based on low cyclic fatigue is still needed.

Ductile failure is cracking damage of the steel material induced by larger cumulative plastic strain under cyclic load. Ductile damage index based on Miner's rule and Manson-Coffin relation can be adopted under earthquakes, as follows (Usami 2007)

$$D_0 = C \sum_{r=1}^n (\varepsilon_{pr})^m \quad (12)$$

where ε_{pr} is the plastic strain range of the very half cycle, and material constants C and m should be obtained by experiments. The two parameters for the steel of this bridge were taken as 9.69 and 1.86 (Ge and Kang 2014). Once the ductile damage index D_0 exceeds 1.0, the ductile failure happens.

Eq. (12) is often used to evaluate the ductile damage at regions with maximum stress of structures. According to Ge and Luo (2011), to consider the influence of stress concentration at column bases, when fiber model is used, a modified factor β is introduced. The ductile damage index applies to fiber models based on low cyclic fatigue is also given as follows

$$D = C \sum_{r=1}^n (\beta \varepsilon_{pr})^m \quad (13)$$

Take column P7 as an example to express the calculation method of β . Establish a fiber model and a shell model of column P7 respectively, as shown in Fig. 22. The fiber model is divided by 5 elements in effective failure length L_e at column base, and the shell model is also finely divided at

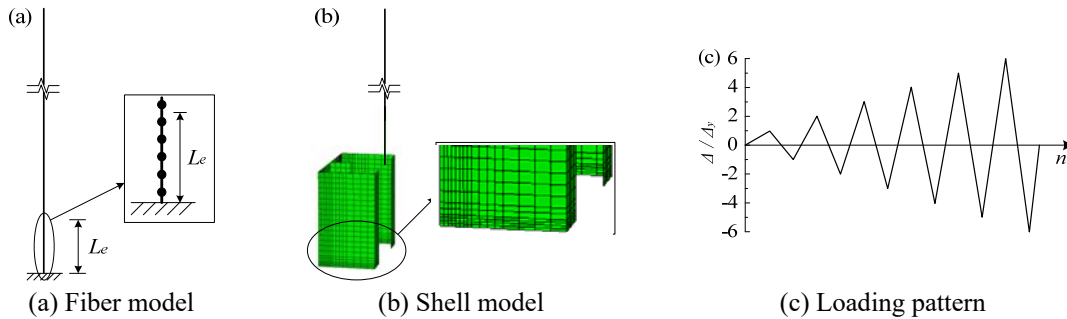


Fig. 22 Calculation of modified factor β

Table 8 Ductile damage index D at damage areas

Section	Chi-Chi Earthquake			Niigata Earthquake		
	D_{I2SM}	D_{M2SM}	D_{BKHM}	D_{I2SM}	D_{M2SM}	D_{BKHM}
Bottom P7	0.08	0.08	0.16	0.73	0.74	0.90
Bottom P8	0.48	0.44	1.26	1.94	1.83	2.78

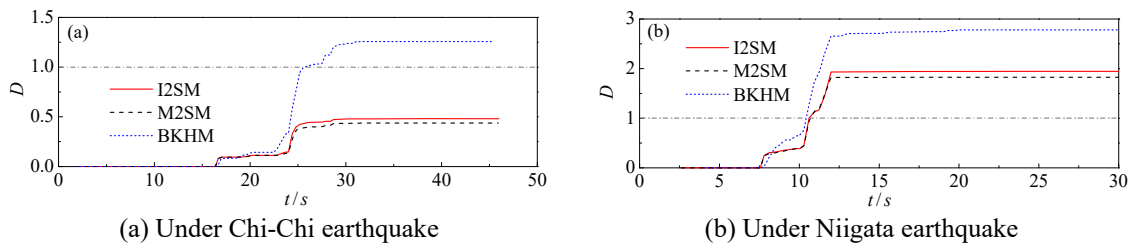


Fig. 23 Ductile damage index D at bottom of column P8

the corners of column base. For the calculation of β , the column was subjected to constant axial load $0.1N_y$ and horizontal cyclic displacement loading Δ at the top, as shown in Fig. 22(c). The shell model is constantly loaded until ductile failure happens (D_0 obtained by Eq. (12) exceeds 1.0). Compare the plastic strain ranges ε_{pr} of each half cycle in the two analyses, the compared integration point is at column base in fiber model, and corner of column base in shell model respectively. β was obtained by averaging the ratios from each half-cycle before ductile failure occurs in shell model. By this means, the obtained β of column P7 and P8 are 2.37 and 2.32 respectively.

Table 8 shows the ductile damage indexes D of severely damaged column P7 and P8. Fig. 23 shows the developing process of damage index D at the bottom of column P8. Results in Table 8 and Fig. 23 demonstrate that in significantly damaged areas, there are large differences between the damage indexes obtained by different hysteretic models, especially at the bottom of P8, where damage index D obtained by BKHM under different ground motions all exceed 1.0. It is far greater than the results of I2SM and M2SM, and leads to completely opposite judgment of ductile failure at the bottom of P8 under Chi-Chi earthquake. Therefore, the effect of hysteretic models on ductile damage index based on low cyclic fatigue in significantly damaged areas should be paid enough attention in structural design and calculation.

5. Conclusions

In this paper, to avoid the defects of unreasonable stress results under complex strain history, the modified two-surface model proposed by Shen *et al.* (1995) was improved on the judgment of stress-strain path. The accuracy and applicability of the improved method were verified on both material and structural level. On the basis of this work, a deck-through type steel arch bridge with a 200m-long span was taken for elasto-plastic seismic response analysis by hysteretic model of I2SM, M2SM and BKHM respectively. The following conclusions can be drawn from this study:

- I2SM could avoid the problem of M2SM in stress calculation when subjected to cyclic loading history with small strain vibrations, and accurately reflects the hysteretic behaviors of the steels.

- Different hysteretic models have relatively small influence on the analysis accuracy of structural seismic displacement responses. The axial force range obtained by BKHM is smaller than that of I2SM and M2SM.

- The damage distributions obtained by the three hysteretic models are similar to each other, but have some difference in dimension. In severely damaged areas, BKHM may underestimate the size of seismic damaged areas.

- Stress-strain responses of the structure are apparently affected by steel hysteretic models. BKHM has smaller stress result than that of I2SM and M2SM, especially in significantly damaged areas.

- The difference between the stress-strain responses obtained by I2SM and M2SM cannot be neglected. In significantly damaged areas, BKHM gives obviously different strain response compared with I2SM and M2SM, and it tends to overestimate the effect of hysteretic energy dissipation.

- The obvious differences of strain response obtained by different hysteretic models may lead to completely different judgment of failure, which has affected structural seismic damage evaluation based on deformation behavior.

- In severely damaged areas, there are large differences between the damage indexes of low cyclic fatigue obtained by different hysteretic models. BKHM substantially overestimates the seismic damage of the structure.

For future work, the anticipated damaged parts of the structures are to be modeled by fine shell elements. This could provide more accurate information for the size and degree of seismic damaged areas.

Acknowledgments

This study was supported by the Natural Science Foundation of China (51378460). The supports are gracefully acknowledged by the authors.

References

- Alvarez, J.J., Aparicio, A.C., Jara, J.M. and Jara, M. (2012), "Seismic assessment of long-span arch bridge considering the variation in axial forces induced by earthquakes", *Eng. Struct.*, **34**, 69-80.
- Cetinkaya, O.T., Nakamura, S. and Takahashi, K. (2006), "A static analysis-based method for estimating the

- maximum out-of-plane inelastic seismic response of steel arch bridges”, *Eng. Struct.*, **28**(5), 635-647.
- Cetinkaya, O.T., Nakamura, S. and Takahashi, K. (2009), “Expansion of a static analysis-based out-of-plan maximum inelastic seismic response estimation method for steel arch bridges to in-plane response estimation”, *Eng. Struct.*, **31**(9), 2209-2212.
- Chavez, H. and Alvarez J.J. (2008), “Seismic performance of a long span arch bridge taking account of fluctuation of axial force”, *The 14th World Conference on Earthquake Engineering*, Beijing, China.
- Chen, X., Ge, H. and Usami, T. (2011), “Seismic demand of buckling-restrained braces installed in steel arch bridges under repeated earthquakes”, *J. Earthq. Tsunami*, **5**(2), 119-150.
- Dalafalis, Y.F. and Popov E.P. (1975), “A model of nonlinearly hardening material for complex loading”, *Acta Mechanica*, **21**(3), 173-192.
- Gao, S. and Ge, H. (2008), “Applicable range of steel constitutive models under cyclic load”, *China J. Highway Trans.*, **21**(6), 69-75. (in Chinese)
- Ge, H. and Kang, L. (2014), “Ductile crack initiation and propagation in steel bridge piers subjected to random cyclic loading”, *Eng. Struct.*, **59**, 809-820.
- Ge, H., Kono, T. and Usami, T. (2004), “Failure strain of steel segments subjected to combined compression and bending and application to dynamic verification of steel arch bridges”, *J. Struct. Eng., JSCE*, **50A**, 1479-1488. (in Japanese)
- Ge, H. and Luo, X. (2011), “A seismic performance evaluation method for steel structures against local buckling and extra-low cycle fatigue”, *J. Earthq. Tsunami*, **5**(2), 83-99.
- Goto, Y., Wang, Q. and Obata M. (1998), “FEM analysis for hysteretic behavior of thin-walled columns”, *J. Struct. Eng.*, **124**(11), 1290-1301.
- Hu, X., Xie, X., Tang, Z., Shen, Y., Wu, P. and Song, L. (2015), “Case study on stability performance of asymmetric steel arch bridge with inclined arch ribs”, *Steel Compos. Struct.*, **18**(1), 273-288.
- Liang, C.Y. and Chen, A. (2010), “A method for examining the seismic performance of steel arch deck bridges”, *Front. Architect. Civ. Eng. China*, **4**(3), 311-320.
- Lu, Z., Ge, H. and Usami, T. (2004a), “Applicability of pushover analysis-based seismic performance evaluation procedure for steel arch bridges”, *Eng. Struct.*, **26**(13), 1957-1977.
- Lu, Z., Usami, T. and Ge, H. (2004b), “Seismic performance evaluation of steel arch bridges against major earthquakes”, Part 2: Simplified verification procedure, *Earthq. Eng. Struct. Dyn.*, **33**(14), 1355-1372.
- Miyoshi, T., Sakimoto, T., Tsuruta, E., Watanabe, H. and Hirota, T. (2003), “Effect of hardening rules of steel on the analysis of cyclic behavior of steel structures”, *J. Struct. Eng., JSCE*, **49A**, 403-413. (in Japanese)
- Morz, Z. (1969), “An attempt to describe the behavior of metal under cyclic loads using a more general work hardening model”, *Acta Mechanica*, **7**(2-3), 199-212.
- Nonaka, T. and Ali, A. (2001), “Dynamic response of half-through steel arch bridge using fiber model”, *J. Bridge Eng., ASCE*, **6**(6), 482-488.
- Shen, C., Mamaghani, I., Mizuno, E. and Usami, T. (1995), “Cyclic behavior of structural steel, II: Theory”, *J. Eng. Mech., ASCE*, **121**(11), 1165-1172.
- Shi, G., Wang, M., Bai, Y., Wang, F., Shi, Y. and Wang, Y. (2012), “Experimental and modeling study of high-strength structural steel under cyclic loading”, *Eng. Struct.*, **37**, 1-13.
- Usami, T. (2007), *Guidelines for seismic and damage control design of steel arch bridges*, Tokyo: Gihodo Shuppan Co. Ltd. (In Japanese)
- Usami T., Gao, S. and Ge, H. (2000), “Stiffened steel box columns. Part 1: Cyclic Behavior”, *Earthq. Eng. Struct. Dyn.*, **29**(11), 1691-1706.
- Usami, T., Lu, Z. and Ge, H. (2005), “A seismic upgrading method for steel arch bridges using buckling-restrained braces”, *Earthq. Eng. Struct. Dyn.*, **34**(4-5), 471-496.
- Usami, T., Lu, Z., Ge, H. and Kono, T. (2004), “Seismic performance evaluation of steel arch bridges against major earthquakes”, Part 1: Dynamic analysis approach, *Earthq. Eng. Struct. Dyn.*, **33**(14), 1337-1354.